ASEAN
Journal of Scientific and Technological Reports
Online ISSN:2773-8752

Academic article

Experimental Investigation of Pitting Corrosion Behavior of 304L Stainless Steel on MnS Inclusions in Chloride Environments Applied to the Mediterranean Industry

Kamel Benlouanas[1, 2*], and Lazhar yahia[3]

[1] Department of Genius-Mechanics, Mohamed Khider University, BP 145 RP, Biskra, 07000, Algeria
[2] Laboratory of Civil and Hydraulic Engineering for Sustainable Development and Environment "LARGHYDE", Mohamed Khider University, BP 145 RP, Biskra, 07000, Algeria
[3] Faculty of Technology, Mostepha Benboulaid University, 53 road of Constantine Fesdis, Batna, 05078, Algeria
* Correspondence: kamel.benlouanas@univ-biskra.dz

Citation:
Benlouanas, K.; Yahia, L.; Experimental investigation of pitting corrosion behavior of 304L stainless steel on MnS inclusions in chloride environments appliced to the mediterranean industry. *ASEAN J. Sci. Tech. Report* **2025**, *28*(5), e258484. https://doi.org/10.55164/ajstr.v28i5.258484.

Article history:
Received: March 27, 2025
Revised: July 17, 2025
Accepted: August 16, 2025
Available online: September 21, 2025

Abstract: Structures made of stainless steel experience a gradual deterioration in their fundamental properties when exposed to both mechanical stress and harsh environmental conditions. This study aims to analyze the impact of cold tensile deformation on the localized roughness corrosion of 304L stainless steel in a 3% NaCl solution, mimicking seawater conditions. Corrosion tests were performed on samples obtained from standardised tensile specimens of the Public Economic Enterprise for the Production of Bolts, Cutlery, and Faucets (BCR) in Boumerdes, Algeria, which had experienced deformation at strain levels of 2.18%, 3.63%, 10.90%, and 16.36%. The results, including corrosion susceptibility, pitting behavior, and repassivation potentials, were evaluated and compared based on the strain. Findings indicate that all measured potentials decrease as the strain increases, except for the roughness potential, which shows a significant decline. This suggests a notable reduction in the material's corrosion resistance with higher deformation levels.

Keywords: Pitting corrosion; 304L stainless steel; effect; deformation; traction

1. Introduction

excellent resistance to uniform corrosion. This corrosion resistance is primarily attributed to the formation of a stable, self-healing passive oxide film on the surface. Among these materials, austenitic stainless steels, such as 304L, offer an optimal balance between mechanical strength, ductility, and corrosion resistance [1, 2]. This study aims to address this gap by experimentally evaluating the effect of cold deformation on the pitting corrosion behavior of 304L stainless steel. Tests were made on specimens of the public economic enterprise for the production of bolts, cutlery, and faucets (BCR) in Boumerdes, Algeria. Corrosion in metals is an electrochemical process where metals return to their thermodynamically stable oxidized state when exposed to oxidizing environments. In steel, iron reacts with oxygen and moisture to form rust, which can detach and expose new surfaces to further corrosion. While general corrosion is relatively predictable, localized corrosion mechanisms such as pitting are more complex and severe.

Pitting corrosion involves the localized breakdown of the passive layer, leading to rapid, concentrated attack at discrete sites. It requires careful study of

electrochemical kinetics, metallurgical microstructures, and mechanical factors. Although the electrochemical behavior of 304L stainless steel in chloride-containing environments has been extensively investigated [3, 4, 5], limited research has addressed how prior cold deformation influences its susceptibility to localized pitting corrosion. The corrosion resistance of stainless steels is mainly due to their chromium content, typically above 10.5%, which ensures the formation of a protective chromium oxide layer. Alloying elements such as nickel stabilize the austenitic structure and improve toughness and ductility. Additions of molybdenum and titanium can further enhance resistance to localized corrosion and high-temperature degradation [6, 7]. However, the passive film in stainless steels is not immune to breakdown. Aggressive ions such as chlorides can penetrate through defects, inclusions, or microstructural heterogeneities, leading to localized film failure. Cold deformation increases dislocation density and residual stress, which can serve as preferential sites for passive film breakdown and pit initiation. Understanding the combined effect of mechanical deformation and corrosive environments is essential for predicting service performance and ensuring structural integrity.

2. Materials and methods

Stainless steel is categorised into five principal types and exists in over one hundred variations. Diverse applications of temperature regulation for austenitic, heat-resistant materials; Ideal for elevated temperatures: ferritic, exhibiting resistance to corrosion and cracking; Martensitic; durable; Duplex (a combination of ferritic and austenitic steel) provides a wide range of options; Semi-austenitic (precipitation-hardened) alloys, composed of aluminium, niobium, and copper, exhibit considerable strength [8, 9]. The advantages of stainless steel include robust corrosion resistance, straightforward and efficient maintenance, durability and strength, aesthetic simplicity, and minimum environmental impact. Stainless steel possesses various disadvantages, including relatively high cost, lack of environmental friendliness, potential for allergic reactions, susceptibility to smudges, and non-biodegradability [10, 11].

2.1 Utilized Material

The material utilised in this study is the austenitic steel 304L, provided and shaped in the form of sheet metal by the company BCR from Bordj M'Nail (Boumerdes), showing its chemical composition [12]:

Table 1. Chemical composition of the sampling

Chemical components (%)						
Fe	Cr	Ni	Si	Mn	Mo	C
Base	18.78	8.80	0.45	1.34	0,27	0.06

2.2 Applied Material

Considered as 18-8 stainless steel, stainless steel 304 (AISI 304) is the most often used variant with 18-20% Cr and 8-10.5% Ni. This 304 is non-magnetic at annealed circumstances, but following cold processing (such as drawing, bending, rolling...), a part of the austenitic structure is changed into a mildly magnetic martensite. AISI 304 material provides high resistance to air corrosion and oxidation. Its high nickel-chrome alloy concentration offers it good corrosion resistance, making it suitable for end use in the food sector [13- 14].

2.2.1 Tensility assays

The tensile trials were conducted using a Zwick-type equipment at the University of Jijel. It features a digital system linked to a computer that facilitates the graphing of tensile curves and yields results like maximum load, elongation at rupture, etc. [15].

2.2.2 Corroding evaluations

Electrochemical studies were done utilising a computer-controlled EG&G Model 283 potentiostat. The I(E) polarization curves were made with Soft CorrIII software.

At the start of the experiment, the metal works as the cathode of the cell. The applied voltage grows positively, and at a predetermined threshold, the metal switches to the anode of the cell. The ensuing corrosion

morphology mimics that of natural corrosion when the specified potential is close to the natural corrosion potential. The cyclic polarization curves obtained (I(E) assist in the identification of corrosion potentials, pitting potentials, and repassivation potentials.

Passivation includes introducing a substantial amount of chromium (Cr) into the steel (> 10.5% by mass). Chromium interacts with the oxygen in the air and generates a coating of chromium oxide, Cr_2O_3: $4Cr + 3O_2 \rightarrow 2\ Cr_2O_3$. The compact, adherent, and protective layer is called the "passive layer" [16-18].

2.2.3 Microscopic rigidity experimentations

Rigidity of an iron specimen, exclaimed. The hardness of a stainless steel sample is a characteristic used to describe materials. In our situation, we measured Vickers hardness [19-20].

2.3 Operating modelling conditions

2.3.1 Tensile experiments

The samples, upon arrival, are cold-rolled sheets with a thickness of 3 mm. The steel plates were cut into standardized specimens at the University of Batna. Figure 1 displays the dimensions of the specimens utilized in our study: the gauge length measures 27.5 cm [21-24].

Figure 2a displays the stress-strain curve derived from 304L steel with a strain of 5 mm/min. In this scenario, the elongation corresponding to the maximum load is 48 mm.

Figure 1. Dimensions of a tensile sampling

We have chosen the following intermediate elongations: 6 mm; 10 mm; 30 mm; and 45 mm, which correspond to strains of 2.18%, 3.63%, 10.90%, and 16.36%, respectively. These strains were computed using the following formula :

$$A\% = \frac{L_f - Li}{L_i}$$

A% : Strain
L_i: Specimen length before deformation
L_f: Specimen length after deformation

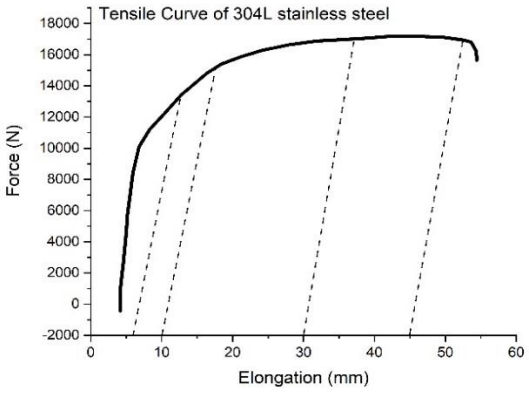

Figure 2a. Conventional tensile curve of 304L steel

2.3.2 Corrosion experiments

For electrochemical investigations, discs of 1 cm2 section were punched out from the usable portion of the specimen that underwent tensile testing. Surface preparation involved polishing with abrasive papers ranging from 600 to 1200 granulometry, followed by fine polishing with a 3 μm diamond paste until a mirror-like finish was reached. Finally, they were cleaned in an ultrasonic immersion containing acetone and dried with compressed air [25-26].

Figure 2b. Evolution of the corrosive state of the 304L stainless steel specimen

Corrosion experiments on these materials were done in a Tacussel CEC/TH three-electrode electrochemical cell, holding 400 ml of 3% NaCl solution, at laboratory ambient temperature, under aerated conditions and without agitation as indicated in Figure 2b. Potentials were measured relative to the saturated calomel electrode (SCE) [27-28].

3. Results and discussion

3.1 Hardness measurement

Mechanical hardness testing is central in the assessment of the mechanical characteristics of iron materials because the hardness values permit one to evaluate the material's resistance to deformation, accompanied by a rough estimation of its hardness parameters, flow stress, among numerous other essential features. Thus, the primary goal of this work has been to create and analyze a computerized approach based on image processing and analysis algorithms that may be employed for determining the Vickers hardness level using hardness strain imaging [29]. The material sample must have a laboratory surface unaffected by fluids, oxidation, flaws, and numerous contaminants to be studied with Vickers hardness. To supply the tester with total faith in the measured results, the experiment's surface must also be smooth and straight. In addition, it is crucial to ensure that the specimen under evaluation has no abnormalities on its contrasting face and that there are no shocks or damages to the testing equipment [30-31].

Figure 3 depicts the fluctuation in hardness as a function of strain rate. This graphic indicates that hardness varies practically linearly with the stress rate. The increase in hardness derives from the degree of work hardening, which increases with the severity of the tensile test [35].

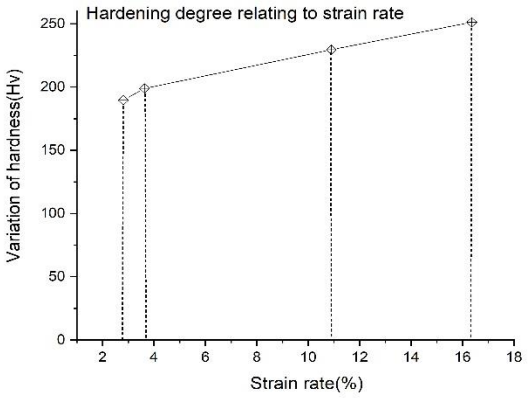

Figure 3. Micrograph sections of 304L stainless steel deformed by tensile : (a) 2.18%; (b) 3.63%; (c) 10.90%; (d) 16.36%.

3.2 Microstructure

These microstructures reveal the polygonal austenite grains with a nanoparticle size and the fully austenitic structure indicative of annealing twins. Microraphs represent the manifestation of strengthening pairs with disarticulated austenitic assembly.

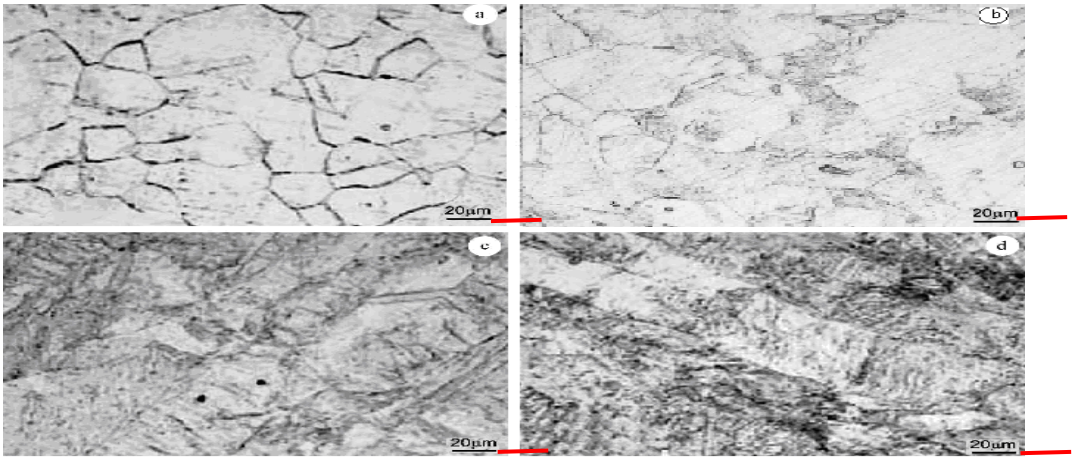

Figure 4. Micrograph sections of 304L stainless steel deformed by tensile (20 µm): (a) 2.18%, (b) 3.63%, (c) 10.90%, (d) 16.36%

The reverted austenite particles and recrystallized small grains, along with untransformed granules, are the essential properties of these microstructures. The quantity of strain-induced martensite has dropped, which is congruent with the reversal cycle already mentioned for X-ray fragmentation studies [32]. A tensile or compressive force that continues across the entirety of a material in the absence of an external load is known as residual stress. Remaining stresses are commonly broken into three categories according to the length scale. Macro-scale stresses, which last for lengthy spans of multiple grain diameters or more, are one category. Macro balance residual stresses indicate ongoing disparity. The change of stainless steel during forming, differential cooling throughout the wall thickness and along the surface during rolling, and localized plastic deformation during handling are common explanations. The other one varies depending on the grain size of the microstructure's morphology [34]. Cold plastic deformation modifies the texture of 304L steel by generating a change in the shape of the grains. During the tensile test, in the plasticity zone, the grains elongate in the direction of the tension. It is noted that the fragmentation into bands and dislocation cells alters the crystal orientation and progressively loses the unique character of the grains (Figure 4).

3.3 Polarization Experiments

From its conception to its most current improvements, the growth of electrochemical potentiokinetic techniques as they correspond to analyzing metals and alloys is followed. These procedures are applied to study the structure and characteristics of stainless steels and some mixed metals, and also for analyzing them for inter-particle corrosion and pitting corrosion in Figure 2b. It is vital to differentiate between polarization graphs associated with particle boundaries and the general structure of the alloy grains (the framework) while studying the propensity of inter-particle and pitting corrosion, applying potentiokinetic polarization tests. Features, potentials, and other properties revealed in the "dual process" analysis may be applied to determine an alloy's ability to undergo intergranular, pitting, and cracking corrosion by periodic polarization tests such as the electrochemical potentiokinetic reactivation (EPR) test. EPR technique for testing enables the capacity of the alloy to pits, intergranular corrosion, and cracking corrosion to be derived from specific characteristics disclosed in the "doubling cycle" test. EPR is rapid to adapt and considers the multiple influences on a material's qualities. The electrochemical potentiokinetic measures can be used for non-destructive testing to clarify the characteristics and responses of materials, as they can sufficiently identify morphological modifications in thermally treated materials that extend beyond stainless steel [35]. The influence of tension deformation on the pitting corrosion behavior of 304L steel was evaluated using the potentiokinetic technique,

by imposing a potential sweep on the sample at a rate of 100 mV/min throughout [-0.45 ~ 0.9 V]. The factors to determine are the corrosion potential (E_c), pitting potential (E_p), and repassivation potential (E_rp). Figure 5 displays a conventional cyclic polarization curve demonstrating these distinct potentials. In our example, we obtain the curves given in Figure 6 for each of the examined strains.

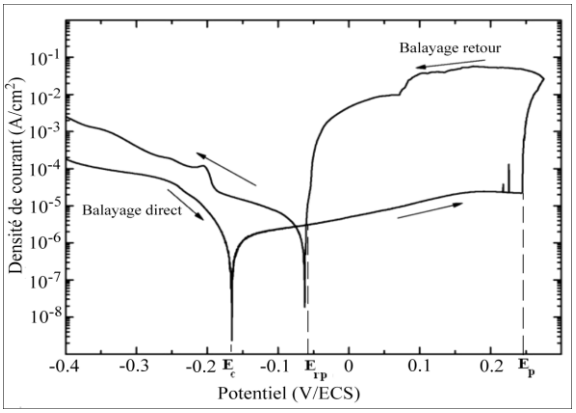

Figure 5. Standard cyclic polarization curve showing the corrosion potential Ec, pitting potential Ep, and repassivation potential Erp

Polarization shapes electrochemical measurements, which can give the needed non-destructiveness, accuracy, duplication, and speed of the process of execution. The polarization curve is a visual picture of the potential propensity link to the corrosion phenomena, which, as a policy, constitutes a steel electrode ensnared in a solution corrosion environment. The roughness of the most fantastic range of corrosion environments is assessed by the polarization trajectory, which also investigates the corrosion pattern of metals and alloys. The rationale for this is that "governed electrochemical polarization" may duplicate a wide range of corrosion processes and phenomena during a given gauging cycle by preserving command of the media's oxidizing strength without needing to move between diverse corrosion contexts. The first thing to know is the type of measurement to reliably distinguish the EPR test from other equivalent processes whose purpose and parameters may be different. This can help you understand an experiment of polarization and to accurately analyze the repercussions of many components, on curves exhibiting more sophisticated shapes.

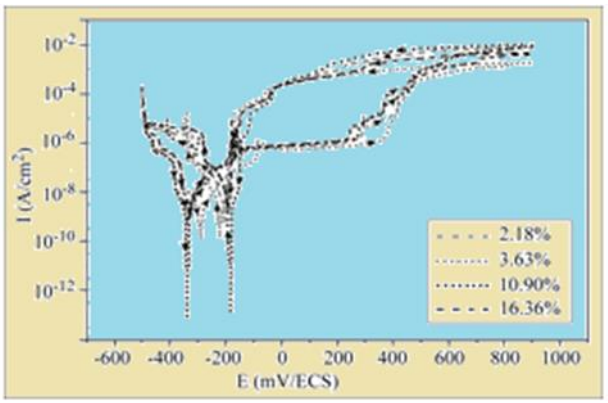

Figure 6. Cyclic polarization curves of 304L steel immersed in 3% NaCl, deformed at various rates by tensile.

The pitting corrosion of 304L stainless steel is tied to the stability of the passive film. This stability takes into account the potential between the metal and the solution. Figure 6 depicts the variability in current density with potential when 304L steel is immersed in 3 % NaCl. Pitting corrosion occurs beyond 0.34 V, in the transpassive domain. A stable pit generated above the pitting potential continues to expand at lower potentials until the repassivation potential; beyond that, repassivation happens. Repassivation potential is

consequently the one below which an already created pit is protected from corrosion, and repassivation is achievable [36]. The modest difference (Ep – Erp) demonstrates valuable resistance to pit growth: the narrower, the more substantial, and the better the corrosion resistance. The breadth of the domain (Ep – Erp) represents the potential of pits to repassivate [37]. Figure 6 led to getting the values of potentials Ec, Ep, and Erp as a function of the varied rates, presented in Table 2. The determination of the domain width (Er – Erp) demonstrates that its extent grows with the increase in the strain. Thus, there is considerable resistance to pit development at low strains.

Table 2. Corrosion, pitting, and repassivation potentials of 304L steel immersed in 3% NaCl at several strains

E (mV) A(%)	Ec	Ep	Erp	Er – Erp	i_{corr} (μA/cm²)	Corrosion Rate (μm/year)
2.81	-320.56	340.36	-130.44	470.80	0.4	4.6
3.63	-360.50	400.20	-140.12	540.32	0.7	8.1
10.90	-380.46	440.10	-150.00	590.10	1.2	13.8
16.36	-420.30	430.45	-200.96	631.41	2.0	23.0

We illustrated the development of these potentials in Figure 7. The corrosion potential tends to drop with increasing strain, making it less noble and more prone to corrosion. The same applies to the repassivation potential, whose decline equates to a decreasing resistance to pitting corrosion. On the other hand, the pitting potential, at the onset of the transpassive domain, tends to decline with the rise in the strain, resulting in a considerable reduction in the passivation domain, as indicated in Figure 6.

3.4 Infinitesimal examinations

The microscope investigations also demonstrated the occurrence of excess non-metallic inclusions on surface samples during corrosion testing. Following corrosion testing, metallographic examinations of the sample reveal that the degree of plastic deformation significantly affects the severity and type of corrosion alterations [38]. Research led to the conclusion that there would be an increase in deformation within the spectrum of a growth in the number, size, and depth of pits. According to acquired assessments, the crack surfaces operate as the anode of a local corrosion cell where metallic degradation takes place. The unstable steel sample underwent microscopic examination, revealing different levels of corrosion resistance in a 3% NaCl solution. A variety of hypotheses have been proposed to describe the stress corrosion phenomena. Of these, stress adsorption and electrochemical dissolution are the two fundamental ideas that have been put out.

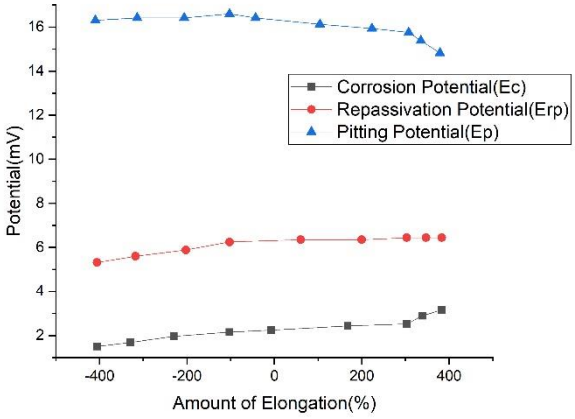

Figure 7. Variation of corrosion, pitting, and repassivation potentials as a function of the strain

The recorded anodized polarization charts indicate the existence of a passive interval. The repassivation potential varies between -130 and -200 mV.

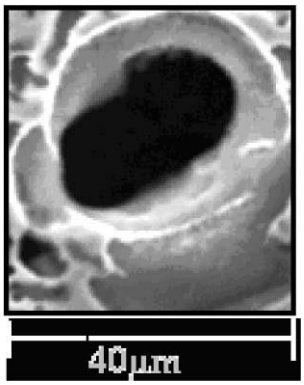

Figure 8. Pitting on the surface of 304L steel micrograph taken by visualizing electron microscopy

The corroded regions of the steel framework are examined microscopically, both before to and following predeformation at various degrees. Interparticular corrosion was identified as the principal source of the corrosion observed in the provided sampling.

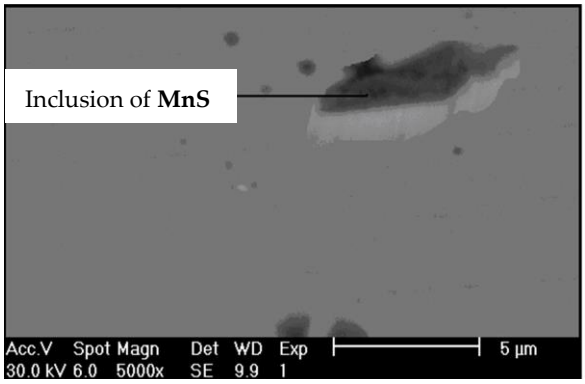

Figure 9. Micrographs obtained by scanning electron microscopy (SEM) showing an MnS inclusion

We conducted electron microscopy to illustrate the shape and scale of the pit dimensions (about 40 µm) (Fig. 8) and to reveal the existence of manganese-based inclusions on the material's surface (Fig. 9). These inclusions may serve as starting locations for pits within the passive coating of stainless steel [39, 40]. Table 1 demonstrates that the material exhibits a substantial manganese content, which leads to the production of manganese sulfide (MnS) inclusions in the presence of sulfur. The presence of MnS functions as a microelectrode when steel is exposed to an aggressive solution such as NaCl. In its vicinity, the passive layer is affected, and the creation of pits is quite possible.

4. Conclusion

This study assesses how surface corrosion deterioration affects the tensile properties of exposed specimens. The damaged experimental specimens were obtained from a model initially exposed to real-world corrosion and subsequently meticulously cleaned on a surface that preserved its original characteristics. In addition to the loss of the authentic piece, the two principal factors that significantly impact strength reduction are the variation in material characteristics due to corrosion and stress concentration resulting from localised rust pits. A comparable stress-strain curve illustrating the corrosion levels of degradation for both preserved and corroded steel plates. The experimental test produced findings indicating the critical fluid media environment of the specimen with an increasing degree of deterioration due to pitting corrosion. This research paper aimed to assess the impact of tensile deformation at varying velocities on the behaviour of 304L stainless steel exposed to a sodium chloride aqueous environment simulating seawater (3% NaCl). The gathered results enable us to draw the following conclusions: the individual character of the grains gradually vanished as the strain reached 10.9%, while the hardness of the steel rose with increasing strain; additionally, the presence of

MnS inclusions created suitable locations for pitting initiation, and the passivation domain diminished with high strains; furthermore, repassivation of pits was more probable for low distortions and generated stronger resistance to local corrosion, whereas the pitting potential tended to diminish with rising strain, resulting in a significant drop in the passivation domain.

5. Acknowledgements

Author Contributions: The authors would like to thank everyone who contributed, directly or indirectly, to the completion of this article from Mohamed Khider University of Biskra and Mostefa Benboulaid University of Batna.

Funding: This research received no external funding.

Conflicts of Interest: The authors declare no conflict of interest.

References

[1] Kaladhar, M.; Subbaiah, K. V.; Rao, C. S. Machining of austenitic stainless steels –a review. *International Journal of Machining and Machinability of Materials* **2012**, *12*(1–2), 178–192.

[2] Peguet, L.; Malki, B.; Baroux, B. Influence of Cold Working on the Pitting Corrosion Resistance of Stainless Steels. *ECS Meeting Abstracts* **2006**, *MA2006-02*(17), 859–859. https://doi.org/10.1149/ma2006-02/17/859

[3] Dhaiveegan, P.; et al. Corrosion behavior of 316L and 304 stainless steels exposed to industrial-marine-urban environment: field study. *Rsc Advances* **2016**, *6*(53), 47314–47324. https://doi.org/10.1039/C6RA04015B

[4] Luo, H.; et al. Effect of cold deformation on the electrochemical behaviour of 304L stainless steel in contaminated sulfuric acid environment. *Applied Surface Science* **2017**, *425*, 628–638. https://doi.org/10.1016/j.apsusc.2017.07.057

[5] Bansod, A. V.; et al. Microstructure, mechanical and electrochemical evaluation of dissimilar low Ni SS and 304 SS using different filler materials. *Materials Research* **2018**, *22*(1), e20170203. http://dx.doi.org/10.1590/1980-5373-MR-2017-0203

[6] Kundu, R. Development of chromium and chromium-nickel electro coated mild steel to enhance corrosion resistance comparable to 304 stainless steel in 3.5% chloride water. **2019**. https://doi.org/10.1016/j.heliyon.2023.e22538

[7] Guo, S.; et al. Corrosion characteristics of typical Ni–Cr alloys and Ni–Cr–Mo alloys in supercritical water: a review. *Industrial & Engineering Chemistry Research* **2020**, *59*(42), 18727–18739. https://dx.doi.org/10.1021/acs.iecr.0c04292

[8] Yu, W.-W.; LaBoube, R. A.; Chen, H. *Cold-formed steel design*; John Wiley & Sons, **2019**.

[9] Scatigno, G. G.; Dong, P.; Ryan, M. P.; Wenman, M. R. The Effect of Salt Loading on Chloride-Induced Stress Corrosion Cracking of 304L Austenitic Stainless Steel under Atmospheric Conditions. *SSRN Electronic Journal* **2019**. https://doi.org/10.2139/ssrn.3441481

[10] Ibrahim, M. Z. A. A. *Developing a new laser cladded FeCrMoCB metallic glass layer on nickel-free stainless-steel as a potential superior wear-resistant coating for joint replacement implants*. Ph.D. Thesis, University of Malaya (Malaysia), **2019**. https://doi.org/10.1016/j.surfcoat.2020.125755

[11] Bellanthudawa, B. K. A.; et al. A perspective on biodegradable and non-biodegradable nanoparticles in industrial sectors: applications, challenges, and future prospects. *Nanotechnology for Environmental Engineering* **2023**, *8*(4), 975–1013. https://doi.org/10.1007/s41204-023-00344-7

[12] Parangusan, H.; Bhadra, J.; Al-Thani, N. A review of passivity breakdown on metal surfaces: influence of chloride-and sulfide-ion concentrations, temperature, and pH. *Emergent Materials* **2021**, *4*(5), 1187–1203. https://doi.org/10.1007/s42247-021-00194-6

[13] Keegan, G. M.; Learmonth, I. D.; Case, C. A systematic comparison of the actual, potential, and theoretical health effects of cobalt and chromium exposures from industry and surgical implants. *Critical reviews in toxicology* **2008**, *38*(8), 645–674. https://doi.org/10.1080/10408440701845534

[14] Linde, G. F. *Investigating the performance of thermal spray coatings on agriculture equipment*. Ph.D. Thesis, Stellenbosch University, Stellenbosch, **2016**.
[15] Moayyedian, M.; et al. Tensile Test Optimization Using the Design of Experiment and Soft Computing. *Processes* **2023**, *11*(11), 3106. https://doi.org/10.3390/pr11113106
[16] Esmailzadeh, S.; Aliofkhazraei, M.; Sarlak, H. Interpretation of cyclic potentiodynamic polarization test results for study of corrosion behavior of metals: a review. *Protection of metals and physical chemistry of surfaces* **2018**, *54*(5), 976–989. https://doi.org/10.1134/S207020511805026X
[17] Bautista, A.; Blanco, G.; Velasco, F.; Gutiérrez, A.; Soriano, L.; Palomares, F. J.; Takenouti, H. Changes in the Passive Layer of Corrugated Austenitic Stainless Steel of Low Nickel Content due to Exposure to Simulated Pore Solutions. *Corrosion Science* **2009**, *51*(4), 785–792. https://doi.org/10.1016/j.corsci.2009.01.012
[18] He, N.; Li, H.; Ji, L.; Liu, X.; Chen, J. Investigation of Metal Elements Diffusion in Cr2O3 Film and Its Effects on Mechanical Properties. *Ceramics International* **2019**, *46*(5), 6811–6819. https://doi.org/10.1016/j.ceramint.2019.11.173
[19] Chicot, D.; et al. Interpretation of instrumented hardness measurements on stainless steel with different surface preparations. *Surface Engineering* **2007**, *23*(1), 32–39. https://doi.org/10.1179/174329407X161573
[20] Cai, Y.; Zheng, H.; Hu, X.; Lu, J.; Poon, C. S.; Li, W. Comparative Studies on Passivation and Corrosion Behaviors of Two Types of Steel Bars in Simulated Concrete Pore Solution. *Construction and Building Materials* **2021**, *266*, 120971. https://doi.org/10.1016/j.conbuildmat.2020.120971
[21] Dobmann, G.; Kern, R.; Wolter, B. Mechanical property determination of heavy steel plates and cold rolled steel sheets by micro-magnetic NDT. In *16th World Conference on Nondestructive Testing (WCNDT)*, **2004**; Fraunhofer-IZFP, Saarbrücken, Germany.
[22] Yu, W.-W.; LaBoube, R. A.; Chen, H. *Cold-formed steel design*; John Wiley & Sons, **2019**. https://doi.org/10.1002/9781119487425
[23] Noronha, D. J.; et al. Deep rolling techniques: A comprehensive review of process parameters and impacts on the material properties of commercial steels. *Metals* **2024**, *14*(6), 667. https://doi.org/10.3390/met14060667
[24] Dehghani, F.; Salimi, M. Analytical and experimental analysis of the formability of copper-stainless-steel 304L clad metal sheets in deep drawing. *The International Journal of Advanced Manufacturing Technology* **2016**, *82* (1), 163–177. https://doi.org/10.1007/s00170-015-7359-9
[25] Jeon, J. H.; Ahn, S.-H.; Melkote, S. N. In Situ analysis of the effect of ultrasonic cavitation on electrochemical polishing of additively manufactured metal surfaces. *Journal of Manufacturing Science and Engineering* **2024**, *146*(4), 041003. https://doi.org/10.1115/1.4064692
[26] Othman, N. H.; et al. The effect of residual solvent in carbon− based filler reinforced polymer coating on the curing properties, mechanical and corrosive behaviour. *Materials* **2022**, *15*(10), 3445. https://doi.org/10.3390/ma15103445
[27] Ogazi, A. C. *Comparative Studies of Electrochemical Corrosion Behaviour of Mild Steel in Some Agro-Fluids*. Ph.D. Thesis, University of South Africa (South Africa), **2015**.
[28] Last, B. A. *Research Concerning the Reference Electrode of the Three Electrode Device for Measuring Corrosion Rates*. **2013**.
[29] Lin, Y.; et al. Mechanical properties and optimal grain size distribution profile of gradient grained nickel. *Acta Materialia* **2018**, *153*, 279–289. https://doi.org/10.1016/j.actamat.2018.04.065
[30] Guo, S.; et al. Corrosion characteristics of typical Ni–Cr alloys and Ni–Cr–Mo alloys in supercritical water: a review. *Industrial & Engineering Chemistry Research* **2020**, *59*(42), 18727–18739. https://dx.doi.org/10.1021/acs.iecr.0c04292
[31] Lingelbach, M. E. Y. *Application of Data Mining and Machine Learning Methods to Industrial Heat Treatment Processes for Hardness Prediction*. Dissertation, **2021**. https://doi.org/10.5445/KSP/1000169018
[32] Vafaeian, S.; et al. On the study of tensile and strain hardening behavior of a thermomechanically treated ferritic stainless steel. *Materials Science and Engineering: A* **2016**, *669*, 480–489. https://doi.org/10.1016/j.msea.2016.04.050

[33] Cios, G.; et al. The investigation of strain-induced martensite reverse transformation in AISI 304 austenitic stainless steel. *Metallurgical and Materials Transactions A* **2017**, *48*(10), 4999–5008. https://doi.org/10.1007/s11661-017-4228-1

[34] Lin, Y.; et al. Mechanical properties and optimal grain size distribution profile of gradient grained nickel. *Acta Materialia* **2018**, *153*, 279–289. https://doi.org/10.1016/j.actamat.2018.04.065

[35] Radojković, B. M.; et al. Non-destructive evaluation of the AISI 304 stainless steel susceptibility to intergranular corrosion by electrical conductivity measurements. *Metals and Materials International* **2024**, *30*(3), 682–696. https://doi.org/10.1007/s12540-023-01536-1

[36] Hadri, F. *l'Université de Lorraine*, France, **2012**.

[37] Stalker, K. *Illustrating pit initiation and evolution in aluminum alloys according to a 3-dimensional cellular automata based model*. Honors Research Project, The University of Akron, **2016**.

[38] Punckt, C.; Bölscher, M.; Rotermund, H. H.; Mikhailov, A. S.; Organ, L.; Budiansky, N.; Scully, J. R.; Hudson, J. L. Sudden Onset of Pitting Corrosion on Stainless Steel as a Critical Phenomenon. *Science* **2004**, *305* (5687), 1133–1136. https://doi.org/10.1126/science.1101358

[39] Park, J. H.; Kang, Y. Inclusions in stainless steels− a review. *steel research international* **2017**, *88*(12), 1700130. https://doi.org/10.1002/srin.201700130

[40] Soltis, J. Passivity breakdown, pit initiation and propagation of pits in metallic materials–review. *Corrosion Science* **2015**, *90*, 5–22. http://dx.doi.org/10.1016/j.corsci.2014.10.006.